# Modeling and image processing for visualization of volcanic mapping

by Maria Teresa Pareschi Ralph Bernstein

In countries such as Italy, Japan, and Mexico, where active volcanoes are located in highly populated areas, the problem of risk reduction is very important. Actual knowledge about volcanic behavior does not allow deterministic event prediction or the forecasting of eruptions. However, areas exposed to eruptions can be analyzed if eruption characteristics can be inferred or assumed. Models to simulate volcanic eruptions and identify hazardous areas have been developed by collaboration between the IBM Italy Pisa Scientific Center and the Earth Science Department of Pisa University (supported by the Italian National Group of Volcanology of the Italian National Research Council). The input to the models is the set of assumed eruption characteristics: the typology of the phenomenon (ash fall, pyroclastic flow, etc.), vent position, total eruptible mass, wind profile, etc. The output of the models shows volcanic product distribution at ground level. These models are reviewed and their use in hazard estimation (compared with the more

<sup>®</sup>Copyright 1989 by International Business Machines Corporation. Copying in printed form for private use is permitted without payment of royalty provided that (1) each reproduction is done without alteration and (2) the *Journal* reference and IBM copyright notice are included on the first page. The title and abstract, but no other portions, of this paper may be copied or distributed royalty free without further permission by computer-based and other information-service systems. Permission to *republish* any other portion of this paper must be obtained from the Editor.

traditional techniques currently in use) is outlined. Effective use of these models, by public administrators and planners in preparing plans for the evacuation of hazardous zones, requires the clear and effective display of model results. Techniques to display and visualize such data have been developed by the authors. In particular, a computer program has been implemented on the IBM 7350 Image Processing System to display model outputs, representing both volume (in two dimensions) and distribution of ejected material, and to superimpose the displays upon satellite images that show 3D oblique views of terrain. This form of presentation, realized for various sets of initial conditions and eruption times, represents a very effective visual tool for volcanic hazard zoning and evacuation planning.

## Introduction

Although less frequent and disruptive than other geological events such as earthquakes and tsunami, and meteorological phenomena such as hurricanes, floods, and droughts, volcanic eruptions have caused vast economic damage and the loss of thousands of human lives. In this century, volcanic eruptions have killed more than 70 000 people and caused an estimated \$10 billion (current value) in property damage. Damage is not strictly related to the size or violence of the eruption, but rather to the proximity of people and productive resources to the volcano. Even a small eruption

in a highly populated region may cause the death of thousands of people.

The goal of planning in volcanic areas is to reduce or minimize volcanic hazard risk. According to the Working Group on the Statistical Study of Natural Hazards [1], risk is defined as the possibility of loss; this includes loss of life, loss of property, loss of productive capacity, etc. From a quantitative point of view, the following relationship can be defined:

 $Risk = (Value) \times (Vulnerability) \times (Hazard).$ 

"Value" can represent the number of lives at stake, or capital value (buildings, land, etc.), or productive capacity (power plants, factories, agricultural lands, etc.). Obviously the value exposed to hazard may change with time as a result either of natural processes or deliberate actions.

"Vulnerability" is that fraction of the value which is likely to be lost as a result of a given event. For the most violent volcanic phenomena (nuées ardentes, lahars, lava flows), the vulnerability of material property is close to 100%, while for ash or pumice falls vulnerability is generally less than 100%. Vulnerability in terms of human lives is more complex to quantify, since it can be reduced by early evacuation from perilous areas.

"Hazard," for volcanic eruptions, is the probability that a particular area will be affected by a destructive eruption in a given time interval. Hazard is a complex function of the probability of eruption and of its typology; it is affected by the quantity, chemical composition, pressure, and temperature of the eruptible magma, by the shape and depth of the magmatic chamber, and by conduit geometry, deep magma feeding, etc.

The estimation of risk, in the present state of knowledge and experience of volcanic eruptions, is a complex task; many of the factors involved, especially those concerning the interior status of volcanoes, are unknown or extremely difficult and costly to obtain.

One realistic approach is to collect data on seismicity, tilt, magnetic field changes, chemical composition and temperature of fluid or solid ejecta, and in general on all those parameters that are reasonably easy to measure which could be "reliable" precursors of dangerous manifestations. The knowledge of such parameters, together with the knowledge of the past eruptive history of the volcano under study, should represent a good starting point. Obviously, there remain the problems of clear interpretation and correlation of these data and of developing reliable methods for using them in the quantitative estimation of hazard.

Whatever the methodology used to estimate hazard, a useful hazard map should be

 Applicable: The dynamics of the eruption must be clear so that adequate assumption about the type of expected eruption, the magnitude of the phenomenon, the location

- of the vent, etc., can be used to predict the distribution of eruption products.
- Reliable: The data base should accurately reflect the distribution of products of past events.
- Flexible: By changing the input parameters according to new data from volcanic surveillance, the techniques of mapping should adequately provide new information.
- 4. Rapid: The hazard maps should be produced in a short enough time to be effective and usable.

Current methods of compiling hazard maps require several years and are primarily based on reconstruction of the eruptive history of a volcano. This approach is useful in identifying areas where high-cost enterprises, buildings difficult to evacuate (e.g., hospitals), etc. should not be located. It is only the first step, however, in assessing the position and extent of areas under risk of impending eruptions.

The goal of this paper is to describe a reliable, more complete methodology. It begins with data derived from monitoring or inferred from the analysis of past eruptive behavior of the volcano under consideration and allows the compilation, that is, the quantitative evaluation and display, of volcanic hazard maps.

## Volcanic eruptions

As noted, a hazard map should be "applicable." This goal is reached when the dynamics of the eruption are well understood, or when the main factors affecting it are identifiable. At the present state of knowledge some kinds of eruptions are well understood, while others are more complex and their physical and chemical behavior less clear. A short note about eruptive behavior may be helpful.

An eruption is initiated when the tensile or shear strength of the overlying rock fails because of magma pressure. Once the volcanic chimney is open (because of excessive magma pressure), magma may ascend and exsolve volatiles (form bubbles). If the gas volume exceeds about 75%, magma disruption (transition from continuous liquid to continuous gas and formation of gas-pyroclast mixture) occurs.

Volcanic eruptions can be divided into two main classes [2]: effusive, consisting of the emission of continuous liquid with scattered bubbles, and explosive, consisting of the emission of fragmented liquids. Within each class, further distinctions can be made according to the different viscosity and volatile content of the magma. The total energy released at the surface during an eruption results primarily from the heat energy contained in solid and liquid products.

Effusive activity generally involves low risk for human life because of the low velocity of the lava. Explosive eruptions (in which a remarkable fraction of energy is transformed into kinetic energy) are characterized by more viscous magmas and higher volatile content and are much more dangerous. Typically these eruptions cause gaseous columns, which

#### Figure

Numerical simulation of the May 18, 1980 Mt. St. Helens tephra fall eruption, showing isomass contours of ash deposition (kg/m²) at the ground level. The model used for simulation is based on a mass continuity equation. Input data are wind profile, atmospheric diffusion coefficients, particle fallout velocities, mass eruption rate, and eruptive column shape.

transport particles from the vent of the volcano into the atmosphere at heights which can reach many tens of kilometers. These are called plinian eruptions; the name comes from the Latin writer Pliny the Younger, who described in the year 79 A.D. the famous eruption of Vesuvius which destroyed the Roman cities of Pompei and Ercolano. If a plume is generated, three regions can be distinguished: the thrust, where the initial momentum is dominant; the convective region, where vertical propulsion results from the density difference between the hot gases and the surrounding cold atmosphere; and the umbrella region, where the gases reach a density equal to that of the surrounding atmosphere and expand to form a mushroom. Solid particles (pyroclastic material), ejected with gases from the vent, follow a path which depends on their size and density. The smallest (tens of microns for pumices) are in thermal and mechanical equilibrium with gases inside the plume, while at a greater distance they are trailed by wind and fall under gravity and form a leeward blanket whose thickness decreases with the increasing distance from the vent. The larger particles (greater than a few centimeters, and relatively heavy) follow ballistic trajectories and settle independently. Particles of intermediate size have a mixed regime. The fallout of pyroclastic products generally does

not involve direct risk of human life, although extensive damage to land and buildings can be expected.

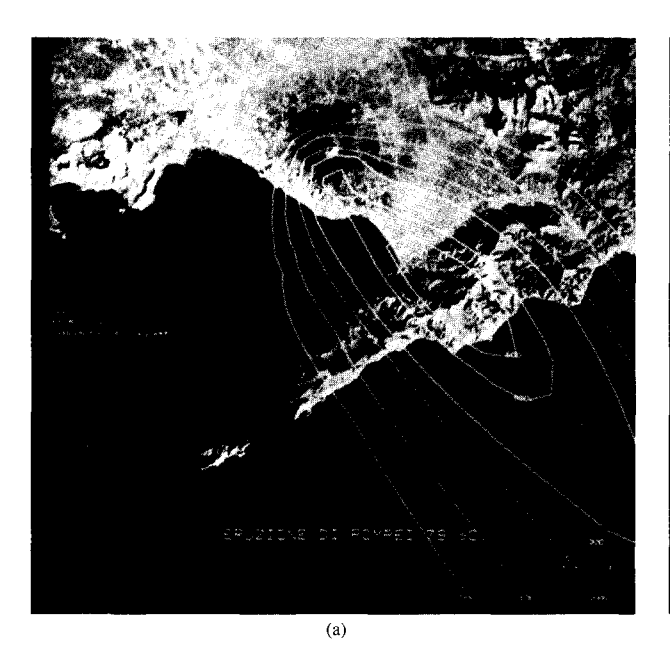
With decreasing velocities, or increasing vent radius, or decreasing gas content, the column may become unable to sustain the solid charge and may collapse, causing very damaging phenomena known as pyroclastic flows and pyroclastic surges. These are emulsions of hot gases and solid particles, fluid enough to flow at great velocity along the volcano slopes. Dilute, highly fluidized particles/gas dispersions are called surges, while dense, incipiently fluidized emulsions are called pyroclastic flows. These phenomena are responsible for the heaviest loss of human life. Thousands of people were killed by the devastating violence of surges and pyroclastic flows at Vesuvius (79, 472, and 1631 A.D.), Mt. Pelée (Martinique, 1902), La Soufrière (St. Vincent, 1902), and El Chichón (Mexico, 1983). Complete destruction can be expected in areas exposed to such eruptions.

# Simulation models and hazard mapping

In recent years, a number of efforts have been made to model volcanic eruptions. The approach is based on the attempt to formulate equations (balance of mass, of momentum, of energy, laws of state) that simulate eruption behavior [3–7]. The system of equations is then solved via numerical methods. Such an approach, if correctly performed, satisfies points 3 and 4 mentioned earlier. Computer-assisted hazard maps are flexible. It is possible to change the initial and boundary conditions of the system of equations (for example, the inferred eruptible mass, the vent position, etc.) and perform a new simulation. The development of faster computers and specialized display hardware allows the solution and visualization of the model outputs in near-real time. Condition 2 is more difficult. As expected, the reliability of the results depends on the capability of the models to adequately describe the physical and chemical behavior of the volcanic phenomena and also on the correct choice of the input parameters. This can be investigated by testing and validating models of past eruptions.

The IBM Pisa Scientific Center and the Department of Earth Science of Pisa University have collaborated since 1984 in developing numerical models that simulate volcanic eruptions to estimate the areas exposed to risk [8]. Since explosive eruptions generally result in a higher risk than effusive phenomena, the starting point of the collaboration was focused on explosive behaviors. Two models have been developed: fallout of volcanic particles (also called "tephra") and pyroclastic surges related to column collapse.

When dealing with tephra fall, there are two distinct phases which must be considered in estimating the path of the particles ejected from the vent of a volcano. The first one is the rise of a column, with its thrust and convective portions. In the second phase, the ash particles leave the



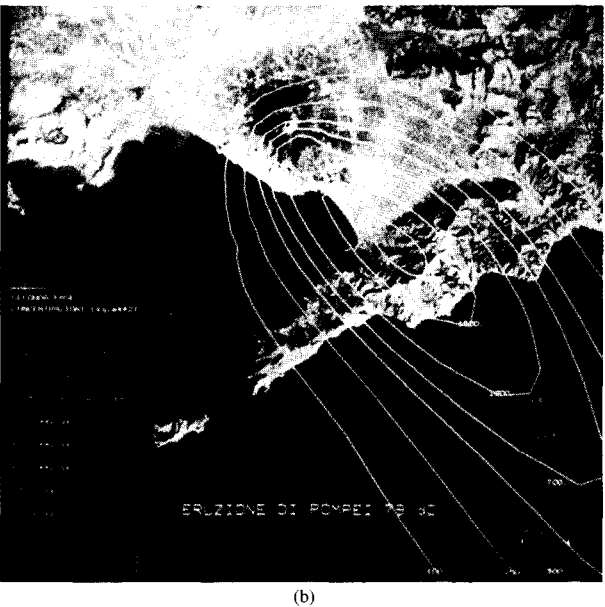


# Figure 2

Reconstruction of the white (a) and grey (b) phases, characterized respectively by the emission of white and grey pumices, of the 79 A.D. plinian eruption of Vesuvius. This eruption caused the destruction of the Roman cities of Pompei and Ercolano. Isomass curves computed by the fallout model at the ground level (kg/m²) are displayed superimposed on a satellite image of the Vesuvian area (pixel resolution 30 m).

cloud under the influence of gravity and are transported by the wind.

Theoretical descriptions and numerical models for the simulation of particle trajectories during the first phase of the eruption have been developed using plume theories or empirical approaches [7–9]. These theories connect column parameters such as density, temperature and pressure of the ejecta, column height, vent radius, column radius, and mass eruption rate.

After the initial plume phase, the paths of the particles are primarily governed by the ambient air currents and can be computed by a continuity mass equation, which, given a negligible vertical wind field, can be written [10, 11] as

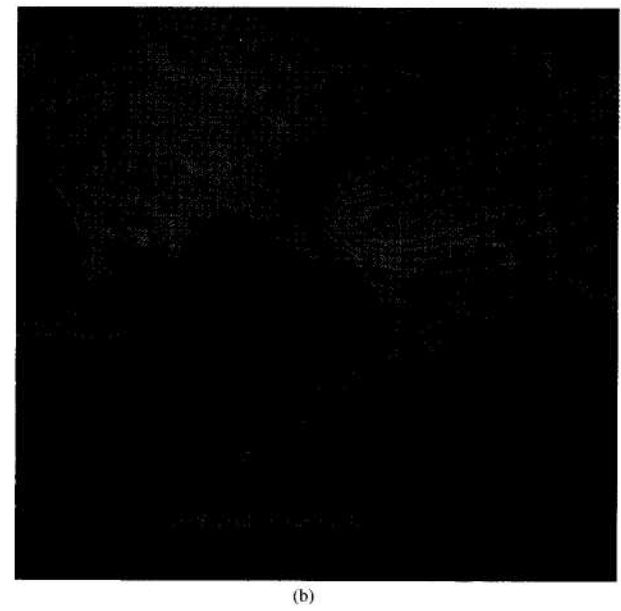
$$\frac{\partial C}{\partial t} + W_x \frac{\partial C}{\partial x} + W_y \frac{\partial C}{\partial y} - \frac{\partial V_s C}{\partial z} 
= \frac{\partial}{\partial x} K_x \frac{\partial C}{\partial x} + \frac{\partial}{\partial y} K_y \frac{\partial C}{\partial y} + \frac{\partial}{\partial z} K_z \frac{\partial C}{\partial z} + S,$$
(1)

where C is the mass concentration of particles,  $W_x$  and  $W_y$  are the horizontal wind components (constant in the x-y plane),  $K_x$ ,  $K_y$ , and  $K_z$  are the diagonal terms of the eddy diffusivity tensor,  $V_s$  is the settling velocity (positive downward), and S is the source (the quantity of particles brought into the system at each instant). This equation holds for each set of particles with an assigned settling velocity, that is, with given grain-size and density. The concentration at ground level (deposition) is given by

$$\int_{T_{-in}}^{T_{\text{max}}} V_{g}C(x, y, z = ground-level \ quote) \ dt, \tag{2}$$

where C(x, y, z = ground-level quote) is the solution of Equation (1) at the ground level,  $V_g$  is the deposition velocity, and  $T_{\text{max}} - T_{\text{min}}$  is the duration of the phenomenon [10, 11]. Equation (1) is numerically solved by splitting it into the advective and the diffusive terms. Advection is solved via the Carlson method; the numerical approximation of diffusion terms is obtained by the method of Crank and Nicolson [10-13]. The reliability of the model has been evaluated and validated by simulating two famous plinian eruptions of the past: the 1980 Mount St. Helens (USA) tephra fall eruption and the 79 A.D. Vesuvius (Italy) plinian eruption. Figure 1 shows the deposition computed by this model for the Mount St. Helens eruption. As in the real case, the model output shows two relative maxima in the pyroclastic deposit on the ground, one near the volcano and another at about 300 km from the vent. The maximum found by the models near the volcano is underestimated. Equation (1) does not fully describe system behavior near the volcano, since other effects such as ballistic ejecta, column collapses, etc. become important here. The second maximum agrees very well with field measurements, both in value (discrepancy <5%) and position (distance about 20 km) [10]. The model has also been tested on the 79 A.D. Vesuvius plinian eruption. Field studies of the volcanic





Computer-assisted reconstruction of a hypothetical fallout eruption at Vesuvius. Isomass lines at ground, in kg/m², are displayed superimposed on a satellite image. The input parameters to the model, which simulates particle transport and fallout in the air, have been inferred from historical considerations and from data obtained by another numerical model which simulates the column behavior above the vent. Results are shown for (a) a winter eruption and (b) a summer eruption. (The results have been obtained by using the most probable average profiles of the winter and summer winds.) It is interesting to note that the Pompei eruption of 79 A.D. happened at the end of August; it corresponds to a summer wind profile with a present-day probability of occurrence of 10%, while the present-day most probable average direction of the summer wind is west-to-east.

deposits of that eruption show that a variety of processes operated during the event. The nature and timing of these processes can be inferred from the physical properties and relative stratigraphic positions of the different eruptive units. Fallout of volcanic particles from a tall column was an important process during most of the eruption, particularly at the beginning. This so-called plinian phase produced a widespread deposit, mantling the local topography and decreasing in thickness downwind from Vesuvius. Accurate observations of this deposit—shape and size, granulometric and density particle distributions, total erupted mass, etc., together with an inferred wind field deduced from analysis of the actual wind field-have allowed a suitable set of input parameters for the model to be defined. The simulation results compare quite well with the field data (discrepancies <10%) [11]. Figure 2(a) shows the first phase of the plinian eruption, characterized by white pumices, while Figure 2(b) shows the second phase, marked by grey pumices.

This model can be used to zone the fallout hazard that would exist if this kind of eruption should happen today at Vesuvius. Careful analysis of available data and some "reasonable" assumptions lead to the hazard maps shown in **Figure 3** [14]. The stronger assumptions are those regarding the total eruptible mass, estimated at about  $2 \times 10^{11}$  kg [15] and the granulometric population (deduced from past

eruptions). Wind field also plays an important role. By averaging data collected over the last ten years [15, 16], the two most probable seasonal wind profiles have been derived (one for summer and the other for autumn-winter-spring). Column height has been computed by the Wilson and Walker column model [7]. Some of the input parameters to that model (eruption duration, vent radius, initial pressure) are not unequivocally determined, resulting in an indeterminate column height of 11–16 km (the isomass lines of Figure 3 refer to a column with a height of 13 km). The considerable variations in the wind profile and column heights involve modifications in the dimensions of the hazardous area. The area inside the isomass line of 50 kg/m², for example, varies from 100 to 300 km².

Model results are a matrix of numbers, each of which gives the tephra deposition on the ground (for example, in kg/m²). Tephra deposition is destructive for buildings at about 100 kg/m², while damage to agriculture is registered at about 50 kg/m². To analyze and exploit such a large amount of data, it is very important to display the results in a visual (or graphical) rather than a mathematical (or tabular) manner.

The fastest and easiest way to achieve a visualization goal is to use satellite image data. From the model results, a set of lines of equal deposition values can be derived and then



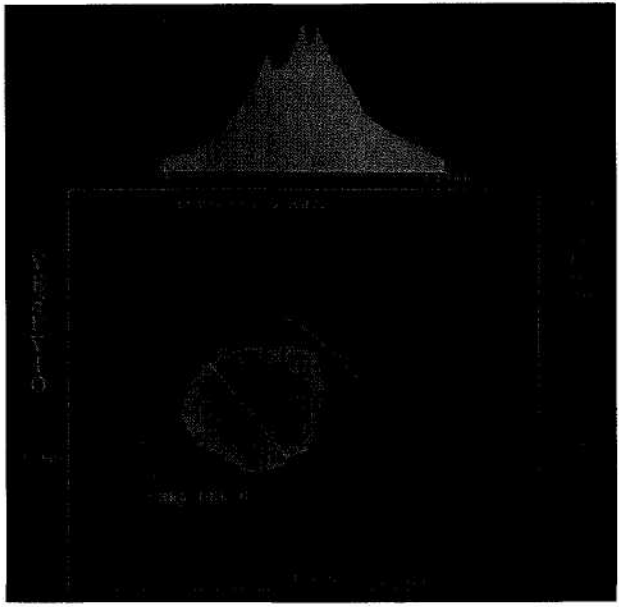
#### Several and Services

Classification of a satellite image (Landsat data) of the Vesuvian area. Classification is a process of assigning the pixels of an image to classes based on the data values in their respective Landsat bands. In the case shown, only one class (urban areas) is computationally selected for visualization. Pixels belonging to that class are displayed in red, while the other pixels retain the original color.

displayed and superimposed onto a satellite image. Landsat images with a pixel resolution of 30 m have been used. Figures 2-4 show some results. These images were displayed on an IBM 7350 Image Processing System.

The use of satellite data provides large-area multispectral coverage of the region of the model results, and shows both natural and cultural features. These data, combined with the model data, provide a realistic presentation of complex model results. Classification algorithms can be used to further categorize and quantify the data (urban areas, agriculture, water, etc.); see **Figure 4**. The relative positions of inhabited zones and zones of dangerous deposition can be rapidly shown.

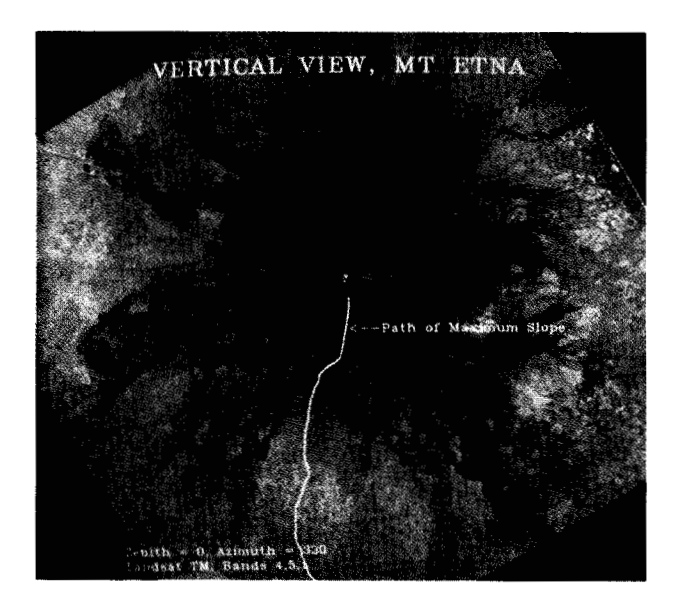
As mentioned, if the column becomes unable to sustain the solid charge, it collapses and the ejected products flow downward over the slopes of the volcano [17]. In this case the initial kinetic energy of the surge or of the flow is due to the potential energy of the erupted column. During the flow, the total energy of the moving products, given by the sum of potential and kinetic terms, decreases continuously because of energy losses due to friction, until the cloud completely stops moving. Malin and Sheridan [6] have proposed to extend the energy line principle, suggested by Hsu to model landslides [18], to pyroclastic surges, by introducing the "energy cone" concept. Energy cone parameters (height related to total initial energy and slope related to energy dispersion due to friction) have been estimated for many



## Figure

Area affected by a hypothetical surge at Vesuvius. The white line shows the maximum distance reachable by the flow. The results are superimposed on a digital terrain map. Different colors represent different vertical heights, or altitudes. In this eruption, topography, together with the initial energy and the coefficients of friction, plays a major role. In the upper part of the image a section (taken along a straight line across the volcano) of the topography and of the deposit thicknesses is shown. Vertical coordinates are exaggerated with respect to horizontal dimensions.

past pyroclastic eruptions [4, 6, 19, 20]. Following Malin and Sheridan, the area of interest is that defined by the line with zero kinetic energy (i.e., the line where the total energy, decreasing with increasing distance from the vent, is equal to the potential energy related to topography). Terrain morphology plays an important role in this phenomenon (Figure 5). For this reason, digital topographic maps of some Italian volcanic areas-Vesuvius, the Phlegraean Fields (a region near Naples), and Etna-have been built [19, 21]. Topographic data have been obtained from maps with a scale of 1:5000 by the Cassa per il Mezzogiorno for the Phlegraean Fields and with a scale of 1:25 000 by IGMI (Istituto Geografico Militare Italiano) for the areas of Vesuvius and Etna. Starting from topographic values taken along contour lines, the map data have been recalculated on a regular grid by a kriging technique [22-24]. The basic concept of this stochastic technique is that the unknown value of a quantity, mathematically expressed by z(x, y), is the realization of an aleatory variable Z(x, y) = t(x, y) + D, where t(x, y) is the local mean value of Z(x, y) and represents the trend, while D is the dispersion around the trend. The estimate  $z_0^{\times}$  of  $z_0$  at the generic point  $P_0(x, y)$  is assumed to be a linear combination of known values  $z_i$  (in



#### 2000 CO (0000)

A path of maximum slope at Mount Etna. The path is computed using information from a digital terrain map of Mount Etna, and the result is displayed on a satellite image (Landsat bands 4, 5, and 1). The path is computed starting from a given point taken, in this case, near the summit of the volcano.

this case, known ground quotes at given points  $P_i$ ):

$$z_0^{\times} = \sum_{i=1}^{N} \lambda_i z_i, \tag{3}$$

where  $z_0^{\times}$  is a realization of the aleatory variable,

$$Z^{\times}(P_0) = \sum_{i=1}^{N} \lambda_i Z(P_i). \tag{4}$$

The weights  $\lambda_i$  of the linear combination are determined in such a way that the error  $E(P_0) = Z(P_0) - Z^*(P_0)$  has a zero mean and a minimum variance:

$$M[E(P_0)] = 0, (5)$$

$$Var\left[E(P_0)\right] = minimum. \tag{6}$$

The kriging technique is preferred over deterministic methods (linear interpolations, splines, etc.) because it ensures the optimization of the estimate and gives the errors for the computed value [Equations (5) and (6)]. The average standard deviation of the calculated quotes is 3 m for the Phlegraean Fields and 10 m for the areas of Vesuvius and Etna.

Digitized topography also plays a major role in lava flows (effusive eruptions). Equations describing a lava path are very complex, because lava is a Bingham fluid, and boundary conditions are very difficult to define [25, 26]. A first intuitive approach to the problem is the computation of

the maximum slope of the topography. Obviously, this gives only an approximate idea of the lava path, since lava itself can constitute a barrier for the oncoming streams when it cools in the open air. The maximum slope is found by using a regression technique. At a given point of the digitized topographic matrix, the nearest 4, 12, 20, etc. neighboring points (each set with a decreasing weight) are used for regression. The number of frames used depends on the topographic resolution. **Figure 6** shows a path of maximum slope at Mount Etna.

If the digitized topography and Landsat image data are available for a given region, the output of the mathematical model can be displayed in a very effective and impressive way. The first step is the registration of the Landsat data and the digital terrain data. Generally, a geometrical transformation must be applied to one of the two images (for example, the satellite image) in order to align and register it with the other image (in our case, the digital terrain data). This operation provides superimposable images. Interactive registration techniques and routines are used to perform these operations [27–31]. Registered digital terrain and Landsat bands can be displayed in perspective; topography gives information on the slope and elevation and Landsat data on the pixel color and class membership [27–36]. The deformation model to apply to perform this transformation is

$$\begin{bmatrix} i' \\ j' \end{bmatrix} = \begin{bmatrix} i'_0 \\ j'_0 \end{bmatrix} + \begin{bmatrix} \cos \psi \cos \phi & & \sin \phi \\ -\cos \psi \sin \phi & & \cos \phi \end{bmatrix} (i-1)s_i + z_i \\ (j-1)s_j + z_j \end{bmatrix},$$

(7)

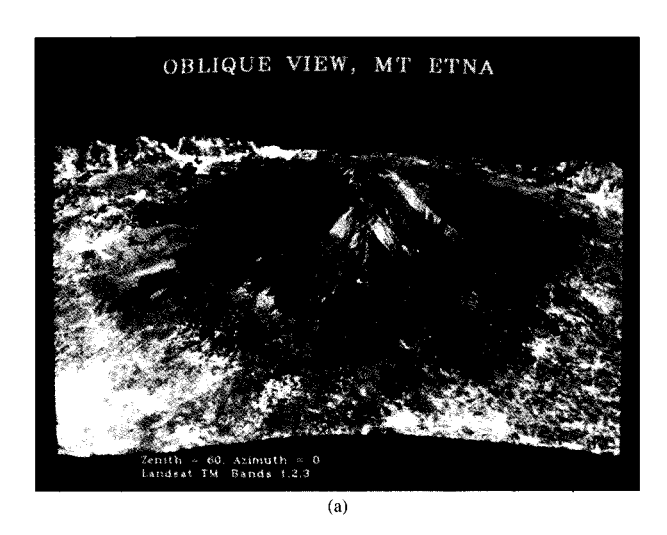
where

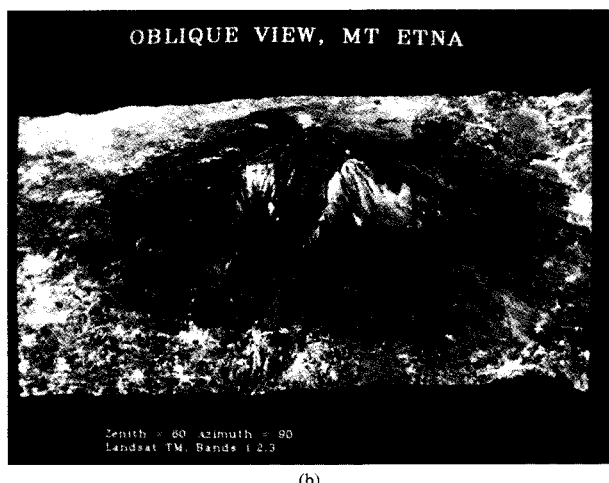
$$\begin{bmatrix} z_i \\ z_i \end{bmatrix} = zxs_z \sin \psi \begin{bmatrix} \cos \phi \\ \sin \phi \end{bmatrix}$$

and (i, j) refers to the input image, (i', j') refers to the perspective image,  $(i'_0, j'_0)$  are the coordinates in the perspective image to which the upper left pixel of the Landsat image is mapped,  $\psi$  and  $\phi$  are the zenith (from the vertical direction) and the azimuth angles, and  $s_i$ ,  $s_j$ ,  $s_z$  are the scaling factors for the i, j, z axes, respectively. The position of the point in the perspective image is computed by using the terrain elevation information at point (i, j), and the point itself is displayed with the color of the corresponding point (i, j) in the Landsat image.

Figures 7-9 show computed oblique views of Mount Etna and the Phlegraean Fields, for different zenith and azimuth angles. Morphological characteristics—vents, ridges, valleys, hills, etc.—can easily be observed by changing the azimuth and zenith angles and by magnifying the vertical scale.

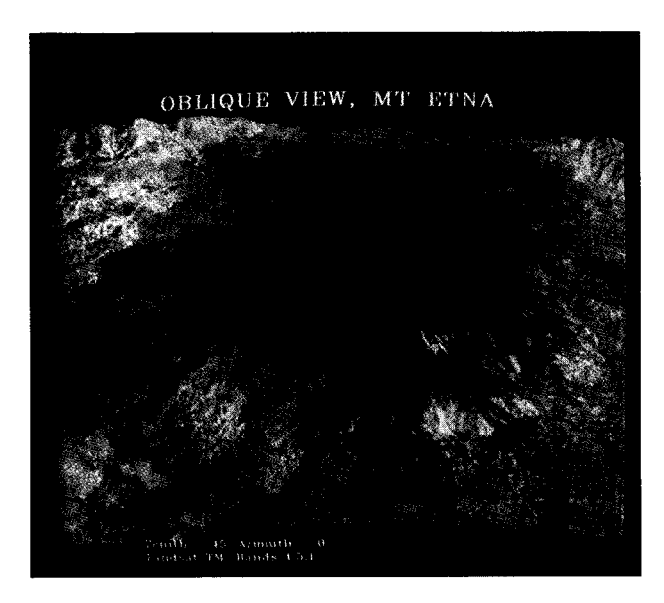
Model outputs can be superimposed on such oblique views. Figure 10 shows a maximum slope path on Mount Etna starting from a point near the top of the volcano. A Landsat image is used as background. A bright stream near the vent of the volcano shows the first stages of the May 1985 lava eruption. The maximum slope is computed by





#### 3

Two oblique views of Mount Etna: (a) azimuth = 0; zenith  $= 60^{\circ}$ ; (b) azimuth  $= 90^{\circ}$ ; zenith  $= 60^{\circ}$ . The representation is obtained from digital terrain data and satellite data (Landsat bands). The digital terrain data provide elevation information, with the azimuth and zenith angles (specified by the user), on the perspective view; Landsat bands 1, 2, and 3 define the color of the pixels.



## a commence

Oblique view of Mount Etna: zenith = 45°; azimuth = 0. Landsat bands 4, 5, and 1 are used to define pixel colors.

James S

Oblique view of the Phlegraean Fields. The vertical dimension is exaggerated with respect to the horizontal scale. Landsat bands 1, 2, and 3 are used to define pixel colors.

starting from a point near the origin of the lava stream. The computed path is localized in Bove Valley.

Figures 11(a) and 11(b) show a hypothetical fallout eruption at two different stages (three hours and nine hours after its beginning) localized at Mount Etna, displayed using 3D views. As shown by these examples, data presented in this format (for different times and initial conditions) could provide planners with a very effective and visual tool for hazard zone evaluation and evacuation planning.

# **Conclusions**

In Italy there are six volcanic areas, the Phlegraean Fields, Vesuvius, Ischia, Etna, Stromboli, and Vulcano, which have erupted in historic times and are therefore considered active.



#### Figure 10

Oblique view of Mount Etna. Landsat bands 4, 5, and 1 are used to define pixel colors. On the slopes of the volcano, a path of maximum slope is depicted. As in Figure 6, the path is computed using a digital terrain map of the volcano, and the starting point is assigned near the summit.

Other volcanic areas that are potentially capable of a renewal of activity include Lipari, Pantelleria, Linosa, and Ustica. The presence of many active volcanoes near densely inhabited areas underscores the necessity of having evacuation plans based on scientifically reliable hazard maps. If an eruption is expected or is ongoing, and some parameters such as wind velocity, source position, and emission rate, etc. can be estimated or inferred, suitable physical-numerical models can compute the extension of the geographical areas under hazard and quantify that hazard in terms of volcanic deposit distribution. To adequately use the outputs of these models, visual display of the predicted results must be rapidly available. A software package has been developed to display model outputs superimposed on digitized topography and on Landsat data. Threedimensional perspective views of the results can also be created by superimposing computational results on Landsat data that have been registered with topographic (digital terrain) data.

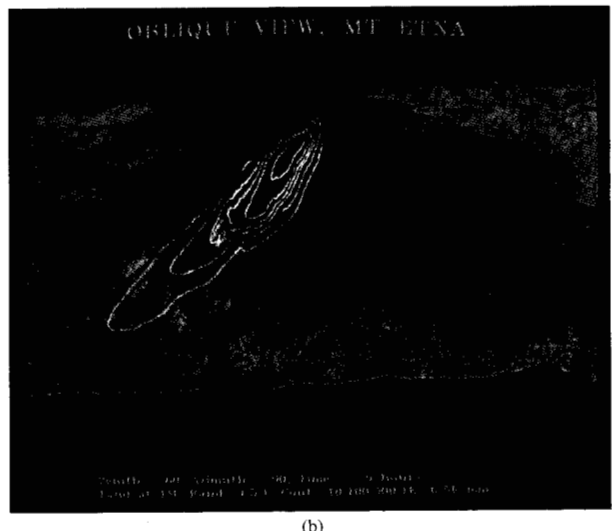
#### References

- Report of Consultative Meeting of Experts on the Statistical Study of Natural Hazards and Their Consequences, Document SC/WS/500, 11 pp., UNESCO, Place de Fontenoy, Paris, France, 1972.
- F. Barberi and P. Gasparini, "Volcanic Hazards," Bull. Intern. Assoc. Eng. Geol. 14, 217–232 (1976).
- S. Carey and R. S. J. Sparks, "Quantitative Models of the Fallout and Dispersal of Tephra from Volcanic Eruption Columns," *Bull. Volcanol.* 48, 109–125 (1986).
- G. Frazzetta, P. Y. Gillot, L. La Volpe, and M. F. Sheridan, "Volcanic Hazard at Fossa of Vulcano: Data from the Last 6,000 Years," *Bull. Volcanol.* 47, No. 1, 105–124 (1984).

- A. T. Hopkins and C. J. Bridgman, "A Volcanic Ash Transport Model and Analysis of Mount St. Helens Ashfall," J. Geophys. Res. 90, No. D6, 10620-10630 (1985).
- M. C. Malin and M. F. Sheridan, "Computer Assisted Mapping of Pyroclastic Surges," *Science*, No. 217, 637–639 (1982).
- L. Wilson and G. P. L. Walker, "Explosive Volcanic Eruptions—VI. Ejecta Dispersal in Plinian Eruptions: The Control of Eruption Conditions and Atmospheric Properties," Geophys. J. Roy. Astr. Soc. 89, 657-679 (1987).
- M. T. Pareschi and R. Santacroce, "Volcanic Eruptions— Mapping the Hazard," *IBM Perspectives in Computing* 8, No. 1, 43-51 (1988).
- T. Suzuki, "A Theoretical Model for Dispersion of Tephra," Arc Volcanism: Physics and Tectonics, D. Shimozuru and I. Yokoyama, Eds., Terra Scientific Publishing Company, Tokyo, 1983. pp. 95-113.
- P. Armienti, G. Macedonio, and M. T. Pareschi, "A Numerical Model for the Simulation of Tephra Transport and Deposition: Applications to May 18, 1980 Mt. St. Helens Eruption," J. Geophys. Res. 93, No. B6, 6463-6476 (1988).
- G. Macedonio, M. T. Pareschi, and R. Santacroce, "A Numerical Simulation of the Plinian Fall Phase of 79 A.D. Eruption of Vesuvius," *J. Geophys. Res.* 93, No. B12, 14817– 14827 (1988).
- R. D. Richtmyer and K. W. Morton, Difference Methods for Initial-Value Problems, Interscience Press, New York, 1967.
- E. Runca, P. Melli, and A. Spirito, "Real-Time Forecast of Air Pollution Episodes in the Venetian Region, Part 1: The Advection-Diffusion Model," *Appl. Math. Modeling* 3, 402–408 (1979).
- 14. G. Macedonio, M. T. Pareschi, and R. Santacroce, "Volcanic Hazard from Tephra Fallout and Flowage During the Next Eruption of Vesuvius," Proceedings of the Kagoshima International Conferences on Volcanoes, National Institute for Research Advancement and Kagoshima Prefectural Government, Japan, 1988, pp. 487–490.
- Government, Japan, 1988, pp. 487–490.

  15. R. Santacroce, Ed., "Somma-Vesuvius," Progetto Finalizzato Geodinamica—Monografie Finali, C.N.R., Quaderni della Ricerca Scientifica 8, 114 (1987).
- W. Cornell, S. Carey, and H. Sigurdsson, "Computer Simulation of Transport and Deposition of the Campanian Y-5 Ash," J. Volcanol. & Geotherm. Res. 17, 89–109 (1983).
- R. V. Fisher, "Models for Pyroclastic Surges and Pyroclastic Flows," J. Volcanol. & Geotherm. Res. 6, 305–318 (1979).
- K. J. Hsu, "Catastrophic Debris Streams (Sturzstroms) Generated by Rockfalls," *Geolog. Soc. Amer. Bull.* 86, 129–140 (1975).
- P. Armienti and M. T. Pareschi, "Automatic Reconstruction of Surge Deposit Thickness: Applications to Some Italian Volcanos." J. Volcanol. & Geotherm. Res. 31, 313–320 (1987).
- M. F. Sheridan and M. C. Malin, "Application of Computer-Assisted Mapping to Volcanic Hazard Evaluation of Surge Eruptions: Vulcano, Lipari and Vesuvius," J. Volcanol. & Geotherm. Res. 17, 187–202 (1983).
- M. T. Pareschi, "Earth Imaging and Data Processing for Mapping and Analysis," in *Digital Signal Processing*, V. Cappellini and A. G. Costantinides, Eds., Elsevier Science Publishers, Netherlands, 1987.
- J. P. Delhomme, "La Cartographie d'une Grandeur Phisique à Partir de Données de Différentes Qualités," *Congr. Hydrogeol.* X, No. 1, 185–194 (1974).
- G. Matheron, "La Théorie des Variables Regionalisées et Ses Applications," Cah. Centre Morphol. Math. 5, Ecoles des Mines. Paris, 1970.
- G. Volpi, G. Gambolati, L. Carbognin, P. Gatto, and G. Mozzi, "Groundwater Contour Mapping in Venice by Stochastic Interpolators. 2. Results," Water Resource Res. 15, 291–297 (1979).
- M. Dragoni, M. Bonafede, and E. Boschi, "Downslope Flow Models of a Bingham Liquid: Implications for Lava Flows," J. Volcanol. & Geotherm. Res. 30, 305–325 (1986).
- G. Hulme, "The Interpretation of Lava Flow Morphology," Geophys. J. Roy. Astr. Soc. 39, 361–383 (1974).





# GITTING A

Oblique views of Mount Etna. Landsat bands 4, 5, and 1 are used to define pixel colors. Two stages of a hypothetical fallout eruption are shown superimposed on the morphology: (a) three hours (zenith 45°, azimuth 0) and (b) nine hours (zenith 60°, azimuth 90°) after the start of the event.

- HLIPS: High Level Image Processing System, IBM Product Offering 5785-ABB, International Business Machines Corporation, October 1984.
- R. Bernstein and D. G. Ferneyhough, "Digital Image Processing," *Photogrammetric Eng. & Remote Sensing XLI*, No. 12, 1465–1475 (1975).
- R. Bernstein, "Digital Processing of Earth Observation Sensor Data," IBM J. Res. Develop. 20, 40–57 (January 1976).
- Ralph Bernstein and William A. Hanson, "Advances in Landsat Image Processing and Mapping," in SPIE Vol. 550, Sensor Design Using Computer Tools II, SPIE—The International Society for Optical Engineering, Bellingham, WA, 1985.
- R. D. Lees, W. R. Lettis, and R. Bernstein, "Evaluation of Landsat Thematic Mapper Imagery for Geological Applications," *Proc. IEEE* 73, No. 6, 1108–1117 (1985).
- J. V. Dave, R. Bernstein, and H. G. Kolsky, "Importance of Higher-Order Components to Multispectral Classification," *IBM J. Res. Develop.* 26, 715–723 (November 1982).
- R. Bernstein, J. B. Lotspiech, H. J. Myers, and H. G. Kolsky, "Analysis and Processing of Landsat-4 Sensor Data Using Advanced Image Processing Techniques and Technologies," *IEEE Trans. Geosci. & Remote Sensing GE-22*, No. 3, 192–221 (1984).
- R. Bernstein, J. B. Lotspiech, and H. J. Myers, "Assessment and New Developments, Jerusalem Conference on Information Technology," Proceedings of the 4th Jerusalem Conference on Information Technology (JCIT), May 21–25, 1984, IEEE, New York, 1984.
- R. Bernstein, J. B. Lotspiech, D. A. Gray, and S. W. Marks, "Interactive Geometric Correction," PASC Report No. 320– 3468, International Business Machines Corporation, October 1984.
- W. Niblack, An Introduction to Digital Image Processing, Strandberg, Denmark, 1985.

Received November 17, 1987; accepted for publication March 15, 1989

Maria Teresa Pareschi IBM Pisa Scientific Center, Via Santa Maria 67, I-56100, Pisa, Italy. Dr. Pareschi received the "Laurea" in physics from the University of Pisa and a special Master's degree in physics at the Scuola Normale Superiore of Pisa in 1978. In 1979 she received a fellowship at ENEA (Ente Nazionale Energie Alternative), where she worked on problems of plasma physics in collaboration with EURATOM; she later received a grant from the Massachusetts Institute of Technology for studies in computational plasma physics. Dr. Pareschi has been working since 1980 at the IBM Scientific Center at Pisa in the area of modeling and image processing, and has written numerous papers in those fields. She is a member of AEEI (Associazione Eletrotecnica e Elletronica Italiana) and the Institute of Electrical and Electronics Engineers.

Ralph Bernstein IBM Palo Alto Scientific Center, 1530 Page Mill Road, Palo Alto, California 94304. Mr. Bernstein is a Senior Technical Staff Member and manager of the Image Science and Applications Department at the IBM Palo Alto Scientific Center. He has a B.S. degree in electrical engineering from the University of Connecticut and an M.S. degree in electrical engineering from Syracuse University. Mr. Bernstein has been involved in image science, applications, and systems development since 1972. His other application experience includes systems simulation and analysis studies for aircraft and submarine navigation and control, satellite systems studies, geophysical data processing, and advanced control systems design. He was responsible for developing the first computerized shipboard oceanographic data acquisition, processing, and control system. Mr. Bernstein was a principal investigator on the NASA Landsat satellite program in 1972-1975 and again in 1982-1985. He developed advanced algorithms and computer programs under these investigations and made significant contributions to the field of image processing. His current interests include visualization and supercomputing, in particular medical, astronomical, and

geophysical image processing. Mr. Bernstein edited the IEEE Press Book Digital Image Processing for Remote Sensing, has contributed to several other books on geoscience and related subjects, and has numerous other publications in geoscience, automatic control, systems simulation, digital image processing, navigation, and oceanography. He served as Chief Imagery Consultant to the National Geographic Society on the publication of their book, Atlas of North America-Space Age Portrait of a Continent. He holds a patent on digital filtering and has several published invention disclosures. Mr. Bernstein is a past member of the Space Science Board and the Space Applications Board of the National Academy of Sciences and has been a consultant to NASA. He is also the Chairperson of the IBM Pattern Recognition and Image Processing Interdivisional Technical Liaison group. He has received the NASA Medal for Exceptional Scientific Achievement, the NASA Public Service Medal, the University of Connecticut Distinguished Alumni Award, an IBM Outstanding Contribution Award, the IBM General Manager's Award for Significant Achievement, and the Tau Beta Pi Eminent Engineer Award. Mr. Bernstein is a Fellow of the Institute of Electrical and Electronics Engineers and a member of the American Society of Photogrammetry and Tau Beta Pi.